A FINITE POINT METHOD FOR ELASTICITY PROBLEMS

E. Oñate, F. Perazzo* and J. Miquel
International Centre for Numerical Methods in Engineering
Universidad Politécnica de Cataluña
Gran Capitán s/n, 08034 Barcelona, Spain
E–mail: onate@cimne.upc.es
Web page: www.cimne.upc.es

* Professor at the Universidad Técnica Federico Santamaría, Valparaiso, Chile.
Visiting Professor at CIMNE

Key words: Finite Point Method, Meshless Method, Elasticity.

Abstract

The basis of the finite point method for the fully meshless solution of elasticity problems in structural mechanics is described. A stabilization technique based on a finite calculus procedure is used to improve the quality of the numerical solution. The efficiency and accuracy of the stabilized finite point method in the meshless analysis of simple linear elastic structural problems is shown in some examples of applications.

1 INTRODUCTION

Mesh free techniques have become quite popular in computational mechanics. A family of mesh free methods is based on smooth particle hydrodynamic procedures. [1,2]. These techniques, also called free lagrangian methods, are typically used for problems involving large motions of solids and moving free surfaces in fluids. A second class of mesh free methods derive from generalized finite difference (GFD) techniques [3,4]. Here the approximation around each point is typically defined in terms of Taylor series expansions and the discrete equations are found by using point collocation. Among a third class of mesh free techniques we find the so called diffuse element (DE) method [5], the element free Galerking (EFG) method [6,7], the reproducing kernel particle (RKP) method [8], the meshless local Petrov-Galerkin (MLPG) method [9,10] and the method of finite spheres [11]. These methods use local interpolations for defining the approximate field around a point in terms of values in adjacent points, whereas the discretized system of equations is typically obtained by integrating the Galerkin variational form over a suitable background grid.

The *finite point method* (FPM) proposed in [12–16] is a truly meshless procedure. The approximation around each point is obtained by using standard moving least square techniques similarly as in DE and EFG methods. The discrete system of equations is obtained by sampling the governing differential equations at each point as in GFD methods.

The basis of the success of the FPM for solid and fluid mechanics applications is the *stabilization* of the discrete differential equations. The stable form found by the *finite calculus* procedure presented in [18–23] corrects the errors introduced by the point collocation procedure, mainly next to boundary segments. In addition, it introduces the necessary stabilization for treating high convection effects and it also allows equal order velocity-pressure interpolations in fluid flow problems [22,23]. This paper extends preliminary successful work of the authors to derive a stabilized finite point method for analysis of solid mechanics problems using the finite calculus approach [24].

The content of the paper is structured as follows. In the next section the basis of the FPM approximation is presented. The concept of the finite calculus (FIC) procedure is detailed next. The discretization of the equilibrium equations in solid mechanics using a stabilized finite point method via the FIC technique is described. The efficiency of the stabilized FPM is verified in several applications to the 2D and 3D analysis of simple linear elastic solids.

1.1   Interpolation in the FPM

Let Ω_i be the interpolation domain (cloud) of a function $u(x)$ and let s_j with $j = 1, 2, \cdots, n$ be a collection of n points with coordinates $x_j \in \Omega_i$. The unknown function u may be approximated within Ω_i by

$$u(x) \cong \hat{u}(x) = \sum_{l=1}^{m} p_l(x)\alpha_l = \mathbf{p}(x)^T \boldsymbol{\alpha} \tag{1}$$

where $\boldsymbol{\alpha} = [\alpha_1, \alpha_2, \cdots \alpha_m]^T$ and vector $\mathbf{p}(x)$ contains typically monomials, hereafter termed "base interpolating functions", in the space coordinates ensuring that the basis is complete. For a 2D problem we can specify

$$\mathbf{p} = [1, x, y]^T \quad \text{for} \quad m = 3 \tag{2}$$

and

$$\mathbf{p} = [1, x, y, x^2, xy, y^2]^T \quad \text{for} \quad m = 6 \quad \text{etc.} \tag{3}$$

Function $u(x)$ can now be sampled at the n points belonging to Ω_i giving

$$\mathbf{u}^h = \begin{Bmatrix} u_1^h \\ u_2^h \\ \vdots \\ u_n^h \end{Bmatrix} \cong \begin{Bmatrix} \hat{u}_1 \\ \hat{u}_2 \\ \vdots \\ \hat{u}_n \end{Bmatrix} = \begin{Bmatrix} \mathbf{p}_1^T \\ \mathbf{p}_2^T \\ \vdots \\ \mathbf{p}_n^T \end{Bmatrix} \boldsymbol{\alpha} = \mathbf{C}\boldsymbol{\alpha} \tag{4}$$

where $u_j^h = u(x_j)$ are the unknown but sought for values of function u at point j, $\hat{u}_j = \hat{u}(x_j)$ are the approximate values, and $\mathbf{p}_j = \mathbf{p}(x_j)$.

In the FE approximation the number of points is chosen so that $m = n$. In this case $\mathbf{C}$ is a square matrix. The procedure leads to the standard shape functions in the FEM [25].

If $n > m$, $\mathbf{C}$ is no longer a square matrix and the approximation can not fit all the u_j^h values. This problem can be simply overcome by determining the $\hat{u}$ values by minimizing the sum of the square distances of the error at each point weighted with a function $\varphi(x)$ as

$$J = \sum_{j=1}^{n} \varphi(x_j)\big(u_j^h - \hat{u}(x_j)\big)^2 = \sum_{j=1}^{n} \varphi(x_j)\big(u_j^h - \mathbf{p}_j^T\boldsymbol{\alpha}\big)^2 \tag{5}$$

with respect to the $\boldsymbol{\alpha}$ parameters. This approximation is termed weighted least square (WLS) interpolation. Note that for $\varphi(x) = 1$ the standard least square (LSQ) method is reproduced.

Function $\varphi(x)$ is usually built in such a way that it takes a unit value in the vicinity of the point i typically called "star node" where the function (or its derivatives) are to be computed and vanishes outside a region Ω_i surrounding the point (Figure 1). The region Ω_i can be used to define the number of sampling points n in the interpolation region. In all numerical examples presented in this paper, the normalized Gaussian weight function $\varphi(x)$ is used. Of course $n \geq m$ is always required in the sampling region and if equality occurs no effect of weighting is present and the interpolation is the same as in the LSQ scheme. A discussion on different possibilities for selecting the weighting function $\varphi(x)$ can be found in [12,13,17].

Standard minimization of eq.(5) with respect to $\boldsymbol{\alpha}$ gives

$$\boldsymbol{\alpha} = \bar{\mathbf{C}}^{-1}\mathbf{u}^h \qquad , \qquad \bar{\mathbf{C}}^{-1} = \mathbf{A}^{-1}\mathbf{B} \tag{6}$$

$$\begin{aligned}
\mathbf{A} &= \sum_{j=1}^{n} \varphi(x_j)\mathbf{p}(x_j)\mathbf{p}^T(x_j) \\
\mathbf{B} &= \big[\varphi(x_1)\mathbf{p}(x_1), \varphi(x_2)\mathbf{p}(x_2), \cdots, \varphi(x_n)\mathbf{p}(x_n)\big]
\end{aligned} \tag{7}$$

The final approximation is obtained by substituting $\boldsymbol{\alpha}$ from eq.(6) into (1) giving

$$\hat{u}(x) = \mathbf{p}^T\bar{\mathbf{C}}^{-1}\mathbf{u}^h = \mathbf{N}^T\mathbf{u}^h = \sum_{j=1}^{n} N_j^i u_j^h \tag{8}$$

where the "shape functions" are

$$N_j^i(x) = \sum_{l=1}^{m} p_l(x)\bar{C}_{lj}^{-1} = \mathbf{p}^T(x)\bar{\mathbf{C}}^{-1} \tag{9}$$

It must be noted that accordingly to the least square character of the approximation

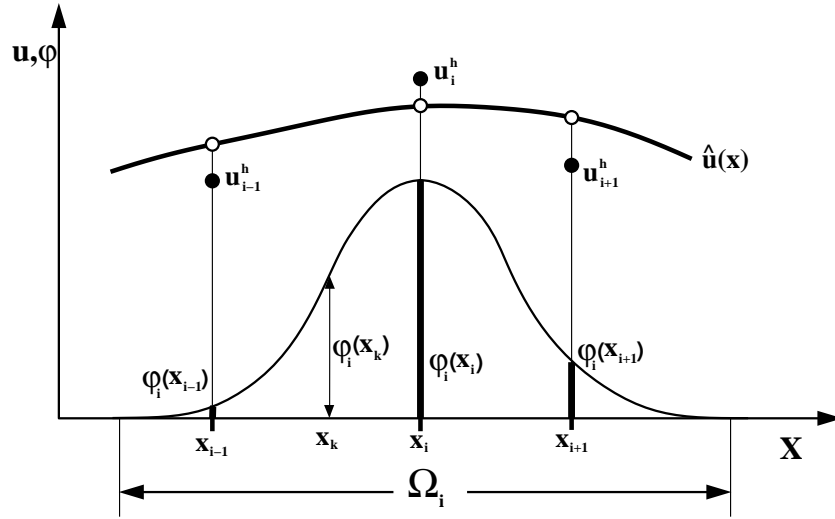$$u(x_j) \simeq \hat{u}(x_j) \neq u_j^h \tag{10}$$

Figure 1: Weighted least square procedure.

i.e. the local values of the approximating function do not fit the nodal unknown values (Figure 1). Indeed $\hat{u}$ is the true approximation for which we shall seek the satisfaction of the differential equation and the boundary conditions and u_j^h are simply the unknown parameters sought.

The weighted least square approximation described above depends on a great extend on the shape and the way to apply the weighting function. The simplest way is to define a fixed function $\varphi(x)$ for each of the Ω_i interpolation domains [13,14,17].

Let $\varphi_i(x)$ be a weighting functions satisfying

$$
\begin{aligned}
\varphi_i(x_i) &= 1 \\
\varphi_i(x) &\neq 0 \qquad x \in \Omega_i \\
\varphi_i(x) &= 0 \qquad x \notin \Omega_i
\end{aligned}
\tag{11}
$$

Then the minimization of the square distance becomes

$$
J_i = \sum_{j=1}^{n} \varphi_i(x_j)(u_j^h - \hat{u}(x_j))^2 \quad \text{minimum}
\tag{12}
$$

The expression of matrices $\mathbf{A}$ and $\mathbf{B}$ coincide with eq.(7) with $\varphi(x_j) = \varphi_i(x_j)$

Note that according to (1), the approximate function $\hat{u}(x)$ is defined in each interpolation domain Ω_i. In fact, different interpolation domains can yield different shape functions N_j^i. As a consequence a point belonging to two or more overlapping interpolation domains has different values of the shape functions which means that $N_j^i \neq N_j^k$. The interpolation is now multivalued within Ω_i and, therefore for any useful approximation a decision must be taken limiting the choice to a single value. Indeed, the approximate function $\hat{u}(x)$ will be typically used to provide the value of the unknown function $u(x)$ and its derivatives in only specific regions within each interpolation domain. For instance by using point collocation

4

we may limit the validity of the interpolation to a single point x_i. It is precisely in this context where we have found this meshless method to be more useful for practical purposes [12–17].

The definition of the points within a cloud for 2D clouds is based on the identification of the points within a circle surrounding each star node. The circle radius is defined so that a minimum number of points is located within the circle domain ($n > 3$ and $n > 6$ for linear and quadratic clouds, respectively, etc.). Obviously, the circle becomes a sphere for 3D clouds.
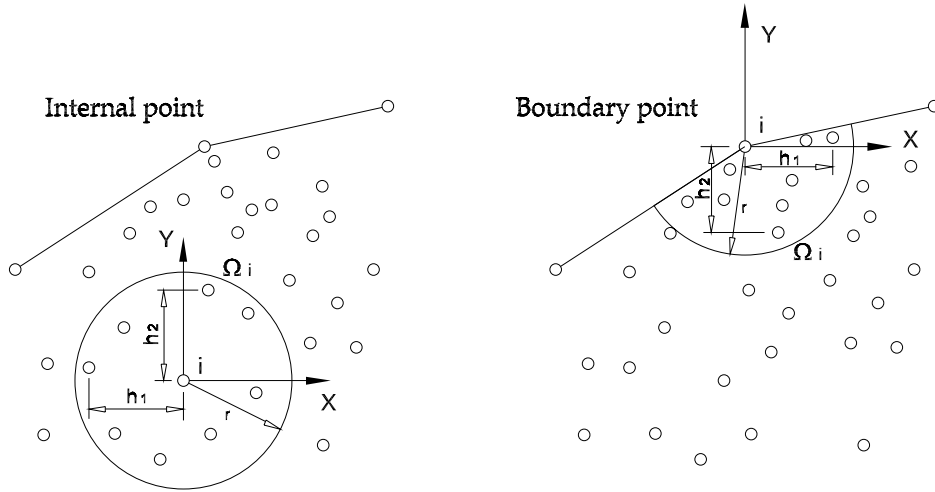
Figure 2: Point search procedure for 2D quadratic clouds and definition of characteristic length distances for interior and boundary points

1.2 Discretization of governing equations

Let us assume a problem governed by the following set of differential equations

$$A(u_j) = 0 \qquad \text{in } \Omega \tag{13a}$$

with boundary conditions

$$u_j - \bar{u}_j = 0 \qquad \text{on } \Gamma_u \tag{13b}$$

$$B(u_j) = 0 \qquad \text{on } \Gamma_t \tag{13c}$$

In above A is a differential operator defining the governing differential equations to be satisfied on the domain Ω with boundary $\Gamma = \Gamma_t \cup \Gamma_\phi$, B is the differential operator defining the boundary conditions at the Neumann boundary Γ_t, u_j are the unknown variables with prescribed values $\bar{u}_j$ at the Dirichlet boundary Γ_u, $j = 1, 2, \cdots, N_v$ where N_v is the number of variables. In solid mechanics applications u_j are the displacements and A and B are the equilibrium equations to be satisfied in the domain Ω and the boundary Γ_t where tractions are prescribed, respectively.

The discretized system of equations in the FPM is found by substituting the approximation (8) into eq.(13) and *collocating* the differential equation at each point in the analysis domain. This gives

$$
\begin{aligned}
\left[A(\hat{u}_j)\right]_p &= 0 \quad, \qquad p = 1, 2 \cdots N_r \\
\left[\hat{u}_j\right]_s - \bar{u}_j &= 0 \quad, \qquad s = 1, 2 \cdots N_u \\
\left[B(\hat{u}_j)\right]_r &= 0 \quad, \qquad r = 1, 2 \cdots N_t
\end{aligned}
\tag{14}
$$

In above N_u and N_t are the number of points located on the boundaries Γ_u and Γ_t, respectively and N_r is rest of the points in Ω not belonging to any of the boundaries Γ_u and Γ_t.

Eqs.(14) lead to a system of algebraic equations of the form

$$
\mathbf{K}\mathbf{u}^h = \mathbf{f}
\tag{15}
$$

where $\mathbf{K}$ is the stiffness matrix, $\mathbf{u}^h$ is the vector collecting the point parameters u_i^h and $\mathbf{f}$ is a vector of known forces acting at the points. Note that, in general, the point collocation procedure leads to a *non symmetric* stiffness matrix [12–16].

In addition, the collocation technique usually leads to an *ill-conditioned system of equations* and the solution of eq.(15) produces unstable and non accurate results. This is mainly due to the incapacity of the point collocation method to satisfy precisely the equilibrium equations over a cloud of points of finite size, just by sampling the equations at the star node in the cloud. Indeed, these deficiencies are more pronounced in clouds next to a boundary segment due to the usual lack of symmetry of the clouds in boundary regions.

The defficiencies of the point collocation procedure can be overcome by using some kind of *stabilization* procedure. This requires the modification of the system of equations (15) in a clever form to avoid the ill-conditioning mentioned above. Most stabilization methods derived for collocation schemes are based on adding to the original equations new terms which are residual-based, i.e. terms which are a function of the governing equations themselves, thus ensuring consistency of the approach. The selection of these terms is somehow heuristic and there is lack of a general stabilization procedure [26].

In our work we have used a stabilized form of the governing equations derived from the Finite Calculus (FIC) procedure described in [18–24]. The FIC method is based on imposing the typical balance laws of mechanics over a domain of *finite size*. The unknown fields are then approximated within the finite domain using a Taylor series expansion, retaining higher order terms than those used in the standard infinitesimal approach. This introduces naturally new terms in the governing differential equations which have stabilization features. The stabilized form of eqs.(13) using the FIC method reads [18]

$$
A - \frac{1}{2} h_k \frac{\partial A}{\partial x_k} = 0 \qquad \text{in } \Omega
\tag{16a}
$$

$$u_j - \bar{u}_j = 0 \qquad \text{on } \Gamma_u \tag{16b}$$

$$B - \underline{\frac{1}{2}h_k n_k A} = 0 \qquad \text{on } \Gamma_t \tag{16c}$$

where n_k are the components of the unit normal to the boundary Γ_t and h_k are the dimensions of the balance domain (also called characteristic length parameters) with $k = 1, 2, 3$ for 3D problems. The underlined terms in eqs.(16a and 16c) introduce the necessary stabilization in the governing equations at discrete level. It is interesting to note that eqs.(16) are the starting point for deriving stabilized finite element methods for advection-diffusion and fluid dynamic problems. Here the new stabilization terms introduced by the FIC technique also account for the instabilities due to convection effects and the incompressibility requirement [18,22,23]. The stabilized equations (16) have also been found useful for enhanced application of the FPM in advective-diffusive transport and fluid flow problems [14–16]. Initial applications of the FIC method for the solution of solid mechanics problems using the FPM were reported in [24]. The underlying ideas of the FIC method have been recently used by Bonet and Kulasegaram to derive stabilized point integrated meshless methods for elliptic equations using SPH techniques [27]. The efficiency of the FIC stabilization procedure for the application of the FPM in elasticity problems is shown in this paper.

The discretized system of stabilized equations in the FPM is found by substituting the approximation (8) into eqs.(16) and *collocating* the differential equations at each point in the analysis domain. This gives

$$\left[A(\hat{u}_j) - \frac{1}{2} h_k \frac{\partial}{\partial x_k} A(\hat{u}_j) \right]_p = 0 \quad , \qquad p = 1, 2 \cdots N_r$$

$$[\hat{u}_j]_s - \bar{u}_j = 0 \quad , \qquad s = 1, 2 \cdots N_u \tag{17}$$

$$\left[B(\hat{u}_j) - \frac{1}{2} h_k n_k A(\hat{u}_j) \right]_r = 0 \quad , \qquad r = 1, 2 \cdots N_t$$

The discretized system of equations (17) can be written in the standard matrix form

$$(\mathbf{K} + \mathbf{K}_s(h_k))\mathbf{u}^h = \mathbf{f} \tag{18}$$

from where the values of the nodal parameters u_i^h can be found.

Matrix $\mathbf{K}$ in eq.(18) denotes the stiffness matrix of eq.(15) excluding the stabilization terms. The effect of these terms is accounted for in the new stabilization stiffness matrix $\mathbf{K}_s$ which is a function of the characteristic length parameters.

The Dirichlet boundary conditions (16b) are introduced in the solution of eq.(18) simply by prescribing the values of the nodal parameters to the fixed displacement values. Indeed this is an approximation as the WLS interpolation does not match the nodal displacement values (Figure 1). A more accurate although expensive procedure can be based in modifying the WLS approximation at the boundary clouds so that the displacement

values at the boundary points satisfy exactly the Dirichlet condition. Further details on the implementation of the Dirichlet boundary conditions can be found in [14,15].

The computation of the characteristic length parameters is a critical issue in order to increase the accuracy of the stabilized solution. An optimum choice of the characteristic length values following a diminishing residual technique can lead to quasi-exact nodal solutions as shown in the FEM analysis of advective-diffusive problems [18–20]. However, for practical purposes stable results can be always found simply selecting the values of the characteristic length distances in terms of the element (or cloud) geometry features. In the examples shown in the paper, the value $h_i = d_i^{\max}$ has been chosen where $d_i^{\max}$ is the largest distance along the ith coordinate axis from a star node in a cloud to its neighbours (Figure 2).

1.3 Stabilized FPM for elasticity problems

Following the ideas presented in the previous section the stabilized equations for elasticity problems can be written as

$$\frac{\partial \sigma_{ij}}{\partial x_j} + b_i - \frac{1}{2} h_k \frac{\partial}{\partial x_k} \left(\frac{\partial \sigma_{ij}}{\partial x_j} + b_i \right) = 0 \quad \text{in } \Omega \tag{19a}$$

$$u_j - \bar{u}_j = 0 \quad \text{in } \Gamma_u \tag{19b}$$

$$\sigma_{ij} n_j + t_i - \frac{1}{2} h_k n_k \left(\frac{\partial \sigma_{ij}}{\partial x_j} + b_i \right) = 0 \quad \text{in } \Gamma_t \tag{19c}$$

with $i, j, k = 1, 2, 3$ for 3D problems. The precise derivation of eqs.(19) can be found in [18].

In above, u_i are the displacements along the cartesian coordinate directions, $\bar{u}_j$ are prescribed displacement values over the Dirichlet boundary Γ_u, b_i and t_i are prescribed body forces and tractions over the domain Ω and the Neumann boundary Γ_t, respectively and σ_{ij} are the stresses which are related to the displacements by the standard Hook's law. In matrix form

$$\boldsymbol{\sigma} = \mathbf{D}\boldsymbol{\varepsilon} \tag{20}$$

where $\mathbf{D}$ is the elastic constitutive matrix and the stress and strain vectors are defined in 3D problems as

$$\boldsymbol{\sigma} = [\sigma_{11}, \sigma_{22}, \sigma_{33}, \sigma_{12}, \sigma_{13}, \sigma_{23}]^T \tag{21}$$

$$\boldsymbol{\varepsilon} = [\varepsilon_{11}, \varepsilon_{22}, \varepsilon_{33}, 2\varepsilon_{12}, 2\varepsilon_{13}, 2\varepsilon_{23}]^T \tag{22}$$

The strains ε_{ij} are related to the displacements by

$$\varepsilon_{ij} = \frac{1}{2} \left(\frac{\partial u_i}{\partial x_j} + \frac{\partial u_j}{\partial x_i} \right) \tag{23}$$

As earlier mentioned h_k are the characteristic length parameters affecting the stabilization terms in eqs.(19a) and (19c). As usual n_k are the components of the unit normal to the boundary.

Note that the stabilization terms require the computation of the third and second derivatives of the displacements in eqs.(19a) and (19c), respectively. This must be taken into account when choosing the order of the interpolation for the displacements.

In our work we have tested the efficiency of the stabilized FPM using quadratic interpolations for the displacement field (i.e. stabilization term in eq.(19a) are zero). The same good results were obtained with the cubic interpolation neglecting the stabilization terms in eq.(19a). This supports the fact that the key stabilization terms are those emanating from the Neumann boundary conditions (eq.(19c)) whereas the stabilization terms in the equilibrium equation on the domain Ω can be neglected for practical purposes. This is also consistent with the nature of the ill-conditioning of the equations due mainly to the lack of symmetry of the points in clouds next to boundary segments.

Examples of the performance of the stabilized FPM in a number of 2D and 3D elasticity problems using quadratic WLS interpolations are shown next.

Example 1. Patch test

The first patch test consists in solving the plane stress equations on a square domain of 2×2 units discretized with 9 points uniformly distributed (Figure 3). A value of $E = 1000$ and $\nu = 0.3$ was taken for the analysis. A prescribed displacement $u = v = x + y$ is assigned to the eight boundary nodes. A quadratic displacement interpolation $(m = 6)$ was chosen for the analysis. The displacements and the stresses computed at the central node coincide precisely with the exact solution. Identical accuracy was obtained by changing the coordinates of the central node as shown in Table 1.
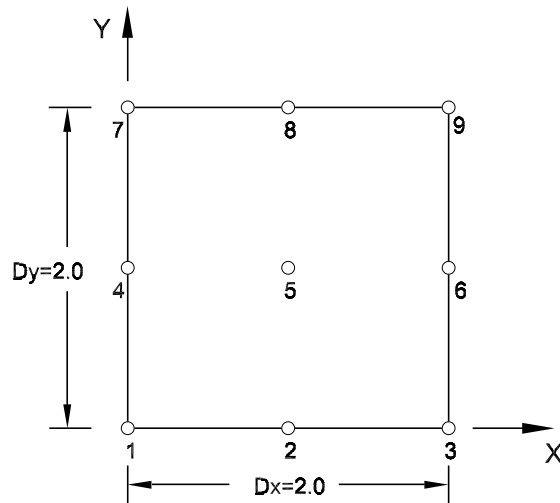

Figure 3: Patch test with regular grid of 9 points

Coordinates of point 5
(1.0,1.0)
(1.2,0.35)
(0.22,0.15)
(1.87,1.9)
Exact values are obtained for the displacements and the stresses at node 5

Table 1: Coordinates of point 5 for the patch test with regular grid of 9 points

The same problem was solved using an irregular grid of 14 points distributed as shown in Figure 4. Again, the exact analytical values for the linear displacement field and the constant stress field are obtained at all the internal nodes (see Table 2).
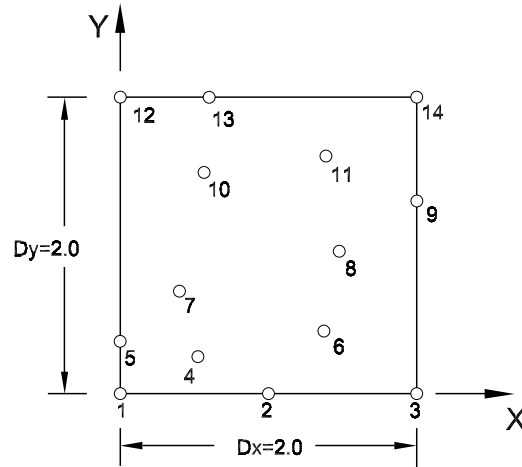
Figure 4: Patch test with irregular grid of 14 points

Points	Coordinates	Displacements $(u = v)$	σ_x	σ_y	τ_{xy}
4	(0.5,0.25)	0.75	0.142857×10^4	0.142857×10^4	0.76923×10^3
6	(1.4,0.45)	1.85	0.142857×10^4	0.142857×10^4	0.76923×10^3
7	(0.38,0.7)	1.08	0.142857×10^4	0.142857×10^4	0.76923×10^3
8	(1.5,1.0)	2.5	0.142857×10^4	0.142857×10^4	0.76923×10^3
10	(0.55,1.5)	2.05	0.142857×10^4	0.142857×10^4	0.76923×10^3
11	(1.38,1.6)	2.98	0.142857×10^4	0.142857×10^4	0.76923×10^3

Table 2: Coordinates and numerical results for a patch test with an irregular grid of 14 points. All numerical results coincide with the analytical values

Example 2. Rectangular domain under prescribed boundary tractions

Figure 5 shows the geometry of the domain, the boundary conditions, the material properties and the discretization into a uniform grid of 28 points. The plane stress assumption was chosen with a unit thickness and values of $E = 1$ and $\nu = 0.25$. The problem was solved for the cases of uniform and linear tractions at the boundary for $x = 6$. The results for the nodal displacements and stresses using the stabilized FPM with quadratic clouds coincide with the analytical values for both loading cases. The horizontal displacement contours for the uniform traction case and the σ_x stress contours for the linear traction case obtained with the stabilized FPM are shown in Figure 6.

a)   b)
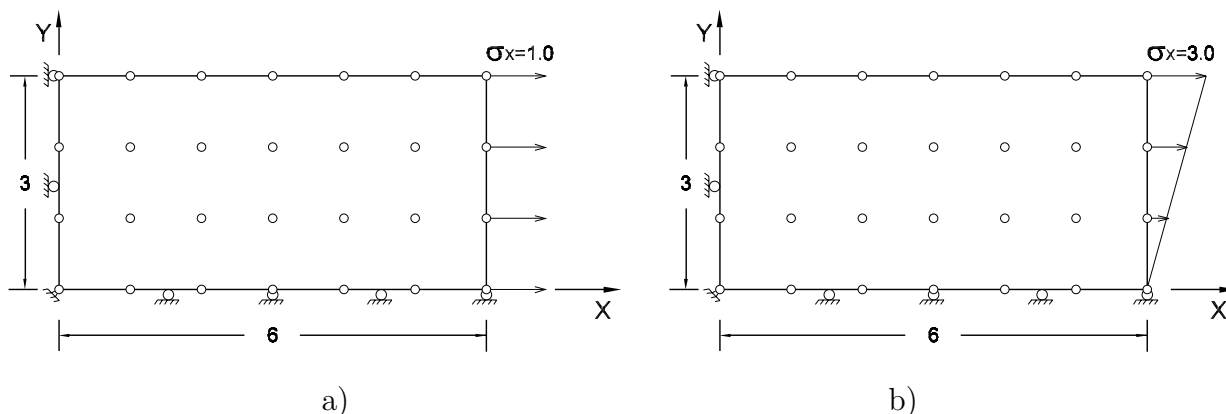
Figure 5: Points arrangement of rectangular domain under prescribed boundary tractions. a) Uniform tractions; b) Linear tractions

a)   b)
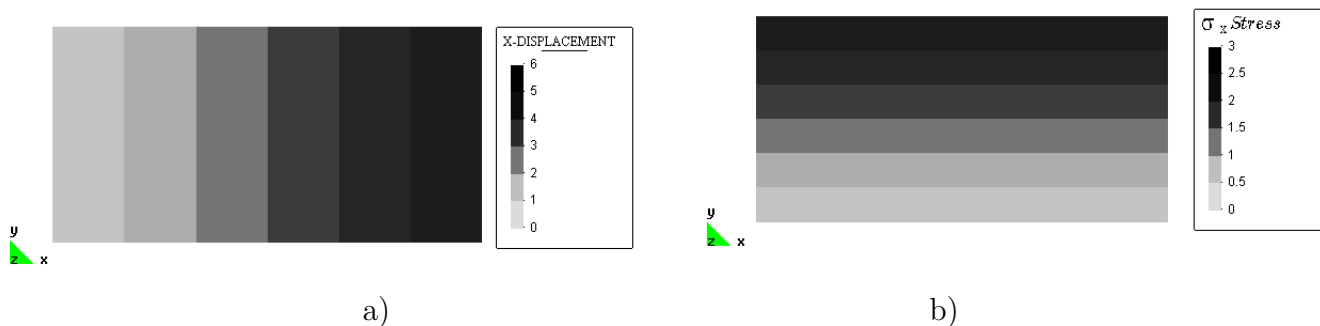
Figure 6: a) Horizontal displacement contours for the uniform traction case; b) σ_x stress contours for the linear traction case

Example 3. Simple supported thick beam under uniform loading

Figure 7 shows the geometry of the beam, the mechanical properties and the uniform distribution of 51 points. A uniform load acting on the upper edge is considered. The problem was solved under plane stress conditions. Once again, a quadratic interpolation

11

for the displacement variables was chosen. Numerical results for the beam deflection and the horizontal stress distribution are shown in Figure 7.
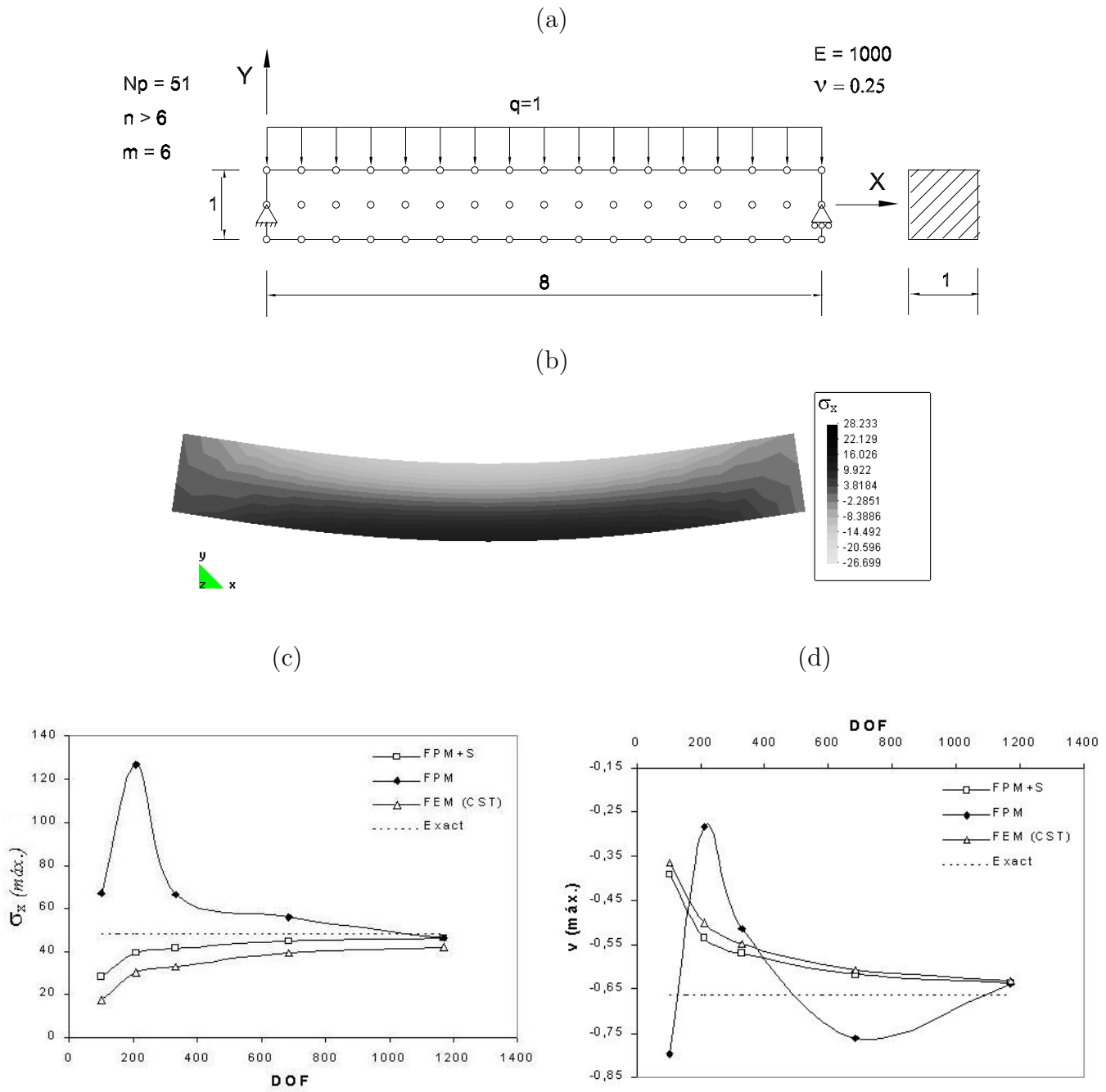

Figure 7: Simple supported beam analyzed with FPM and CST finite elements. (a) Beam geometry, loading and regular grid of 51 points; b) Horizontal stress contours; c) Convergence of the maximum horizontal stress and d) Convergence of the central deflection with the number of degrees of freedom (DOF). Exact solution refers to classical beam theory [28]

12

The same problem was analyzed with the FEM using a structured mesh of 68 linear plane stress triangles (CST element) [25] based on the same point distribution. Nodal stresses have been obtained by standard nodal averaging of element values. Comparison of the errors for the central deflection and the maximum σ_x stress gives some advantage to the stabilized FPM results (see Table 3).

Numerical results for grid of 51 points (68 CST finite elements)			
Central deflection error		Error in maximum σ_x stress	
FPM+S	FEM	FPM+S	FEM
19%	21%	19%	38%

Table 3: Simple supported beam. Numerical results for grid of 51 points (68 CST finite elements)

The convergence of the maximum horizontal stress and the maximum deflection value with the number of degrees of freedom is shown in the lower part of Figure 7, respectively. Results, labelled as FPM+S, correspond to those obtained with the stabilized FPM described in the paper, whereas those listed as FPM were obtained neglecting the stabilization terms (i.e. the terms involving the characteristic lenght parameters in eq.(17)). Note the benefitial effect of the stabilization terms leading to results which are more accurate than those obtained by the standard FEM in this case.

Example 4. Square domain with circular hole under tension

Figure 8 shows the geometry of the domain and the loading. One quater of the domain is analyzed only due to symmetry. Plane strain conditions were assumed for the analysis. The problem has been solved with the quadratic FPM using two unstructured grids of 36 and 60 points. Contours of the horizontal stress obtained with the stabilized FPM are shown for the two grids. Results for the maximum horizontal stress at the upper tip of the hole obtained with the stabilized FPM compare well with the analytical value of $\sigma_x = 3.0$ [28]. The FPM results also compare very favourably with those obtained with the FEM using an unstructured mesh of CST elements (Table 4). The distribution of the maximum horizontal stress along the line $x = 0$ is also shown in Figure 8 for the two grids studied. Note the greater accuracy of the stabilized FPM solution versus the standard FPM and FEM solutions.
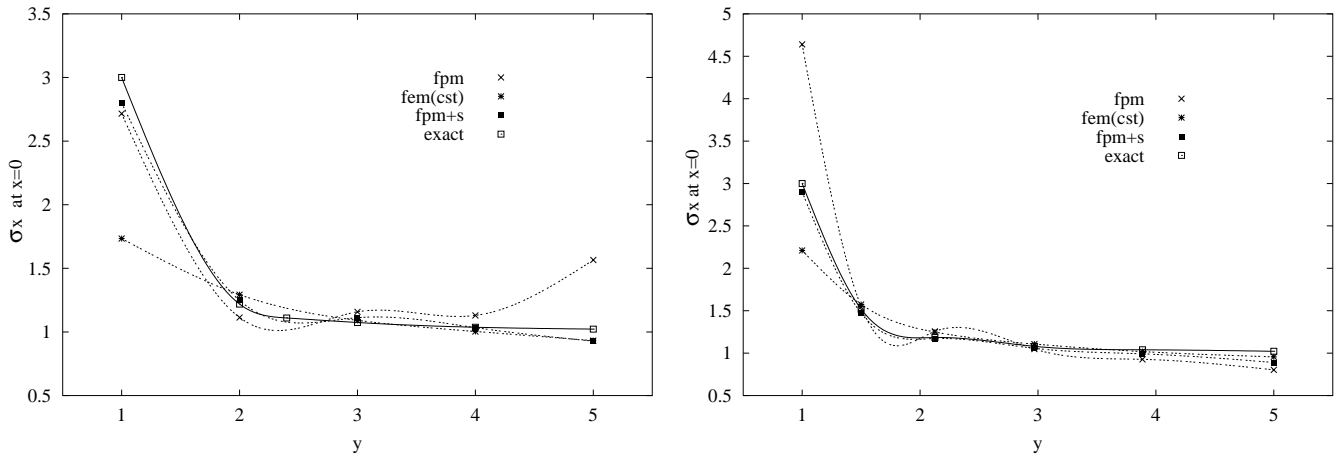
The distribution of the horizontal stress along the line $x = 0$ for the two unstructured grids studied is shown in Figure 9.

a)
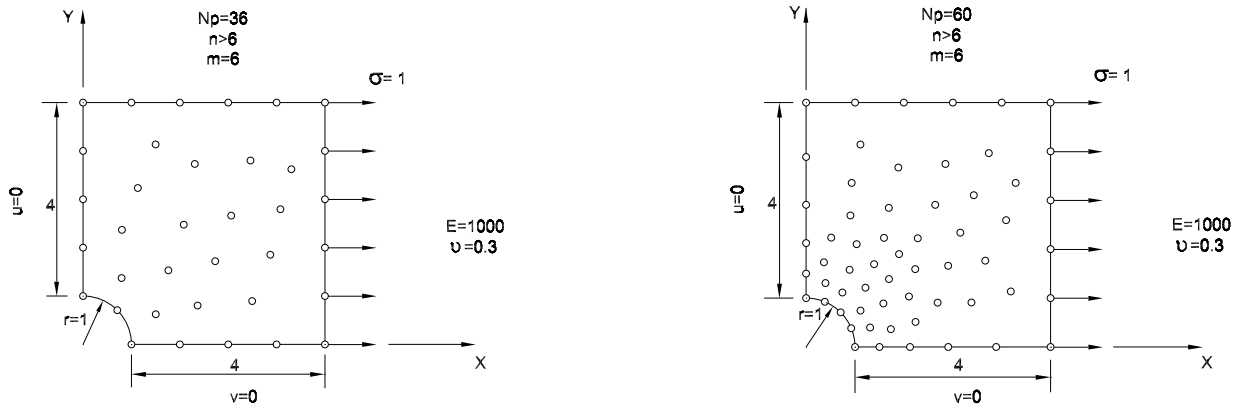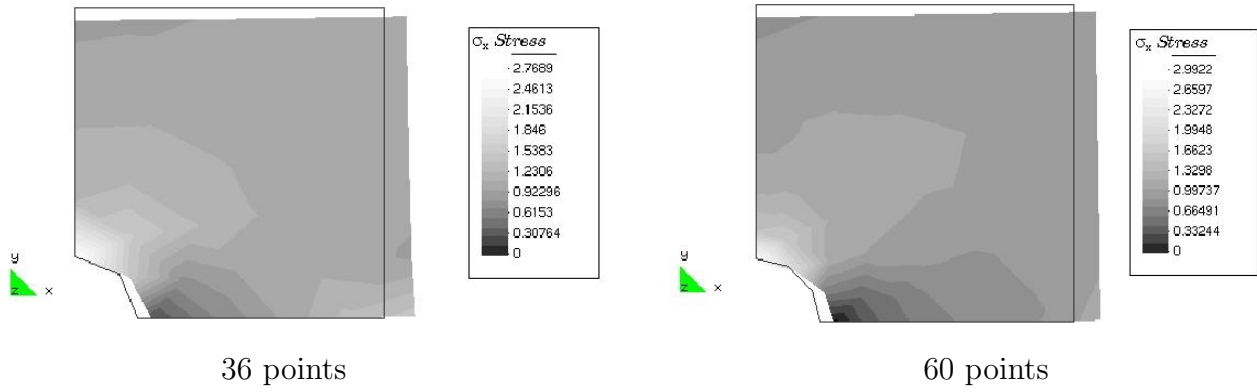
36 points   60 points

b)

c)

Figure 8: Square plate with a circular hole under tension analyzed with FPM and FEM (CST elements) ($E = 1000$, $\nu = 0.3$). a) Plate geometry and loading. Unstructured grids of 36 and 60 points; b) σ_x stress contours displayed over the deformed shapes obtained for the two grids studied; c) Distribution of maximum horizontal stress along the line $x = 0$ for the two unstructured grids of 36 and 60 points

14

36 points - 50 CST Triangles		60 points - 94 CST Triangles	
FPM+S	FEM	FPM+S	FEM
6%	38%	1,5%	21%

Table 4: Square plate with circular hole. Error in the maximum horizontal stress obtained with the stabilized finite point method (FPM+S) and the finite element method (FEM)
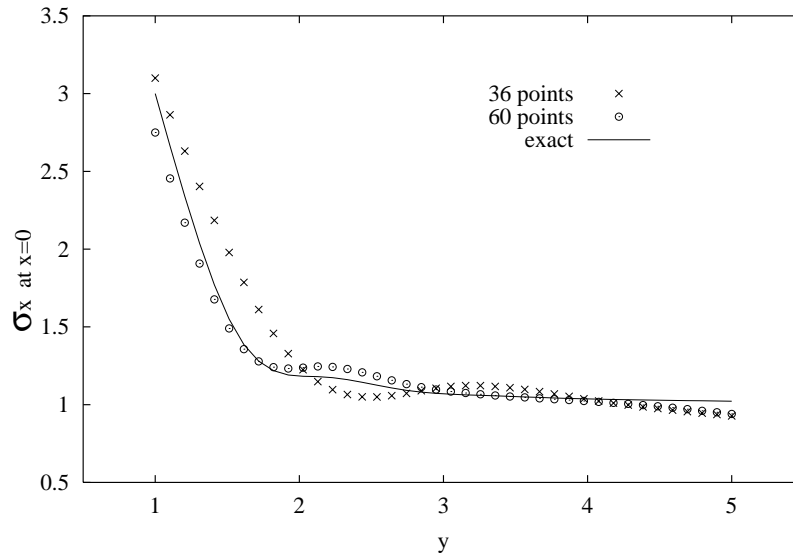
Figure 9: Square plate with circular hole. Distribution of the horizontal stress along the line $x = 0$ for the grids of 36 and 60 points. The exact distribution is also plotted [28]

Example 5. Thick cantilever under end point load

Figure 10 shows the geometry of the cantilever beam and the material properties. The end load of $P = 1.0$ was applied as a parabolic tangential stress acting at the boundary for $x = 8.0$. Plane stress conditions were assumed.

The problem was solved with regular and irregular grids of 55, 165 and 333 points using quadratic clouds. The distribution of points for the regular and irregular grids of 55 points are shown in Figure 10. The contours of the vertical displacement and the σ_x stress obtained with the regular grid of 333 points are plotted in Figure 11. Very similar results were obtained using an irregular grid.

Figure 12 shows a plot of the shear stress distribution at the beam center obtained with the different regular grids. The convergence of the displacement and the σ_x stress using regular and irregular grids is plotted in Figures 13 and 14. The error was measured by the quadratic norm of the differences between point values and the exact solution. Distance h in Figures 13 and 14 denotes to the average radial distance for all the clouds in a grid. The slope of the convergence curves for the displacements u and v are found to be uniform and
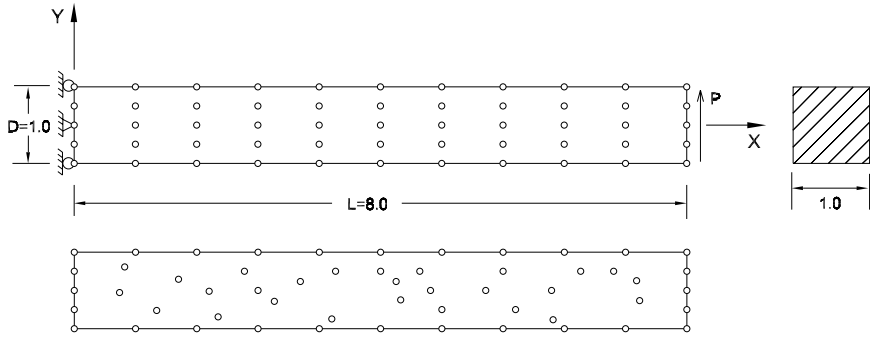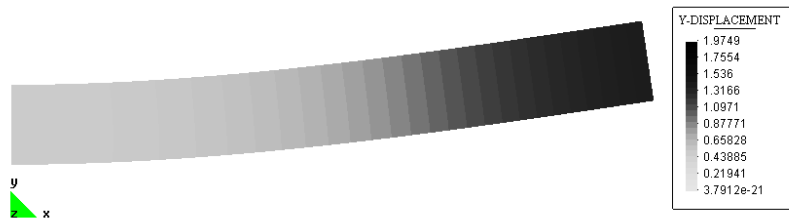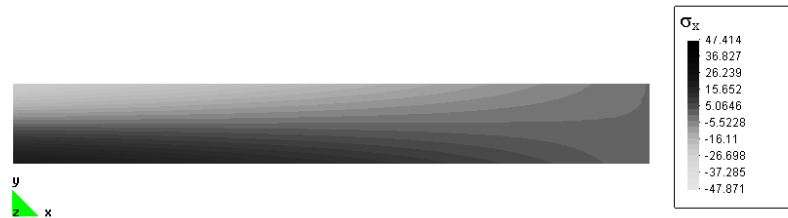
15

Figure 10: Cantilever beam. Regular and irregular grids of 55 points

a)

b)

Figure 11: Cantilever beam analyzed with a regular grid of 333 points. a) Contours of the vertical displacement; b) Contours of the σ_x stress

$\simeq 2$ for regular grids and $\simeq 3$ for irregular grids. It is remarkable that similar convergence rates are obtained for the σ_x stress for both regular and irregular grids.

Example 6. 3D prismatic solid under end bending moments

Figure 15 shows the geometry of the prismatic solid and the material properties. The end bending moments were modelled by an equivalent linear traction acting at the ends. An eight of the solid was analyzed only due to symmetry. A regular grid of $6 \times 5 \times 4$ points was chosen as shown in Figure 15. Figure 16 shows contours of the displacement along the longitudinal z axis and the σ_z stress. A comparison of relevant displacement and stress values with the analytical solution obtained from [28] is presented in Table 5.
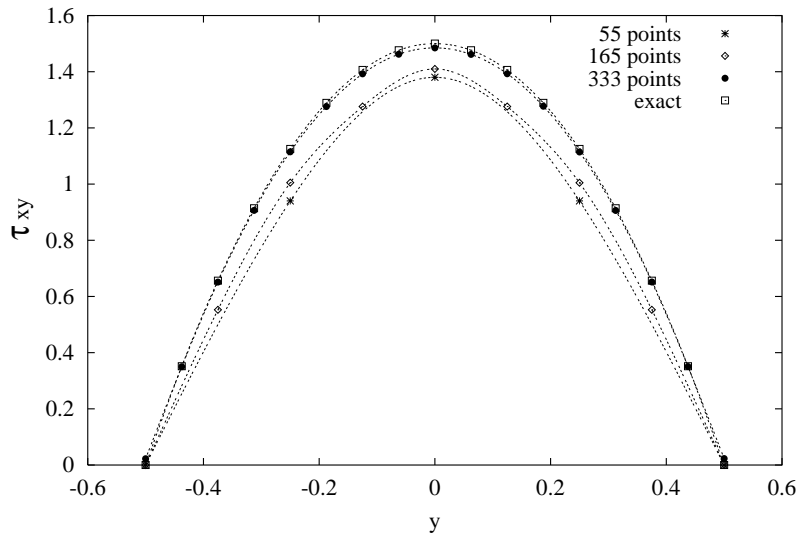
Figure 12: Cantilever beam. Convergence of the shear stress distribution at $x = L/2$ for different regular grids
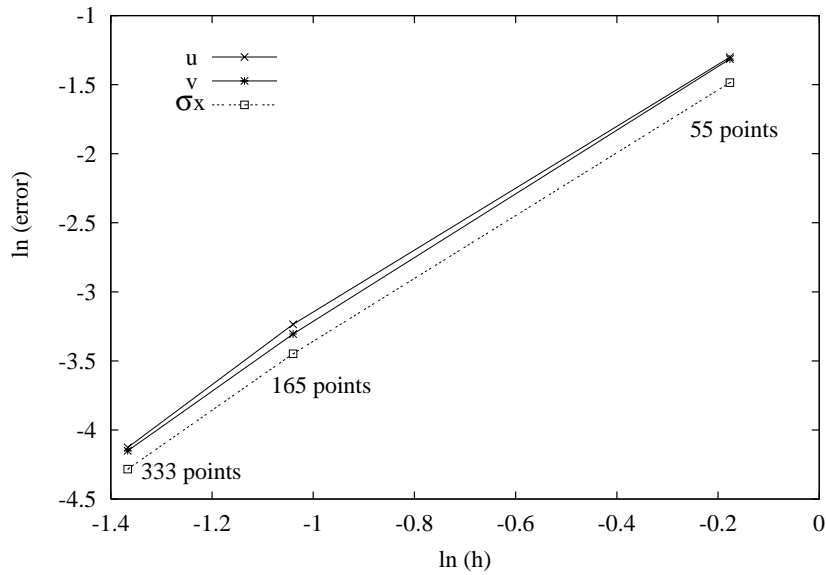

Figure 13: Cantilever beam with regular point distribution. Convergence of displacements and σ_x stress with the average radial distance for all clouds

Finally, Figure 17 shows the contours of the displacement along the z axis and the σ_z stress obtained *without the stabilization terms*. Note that the solution drastically deteriorates in this case, as expected.
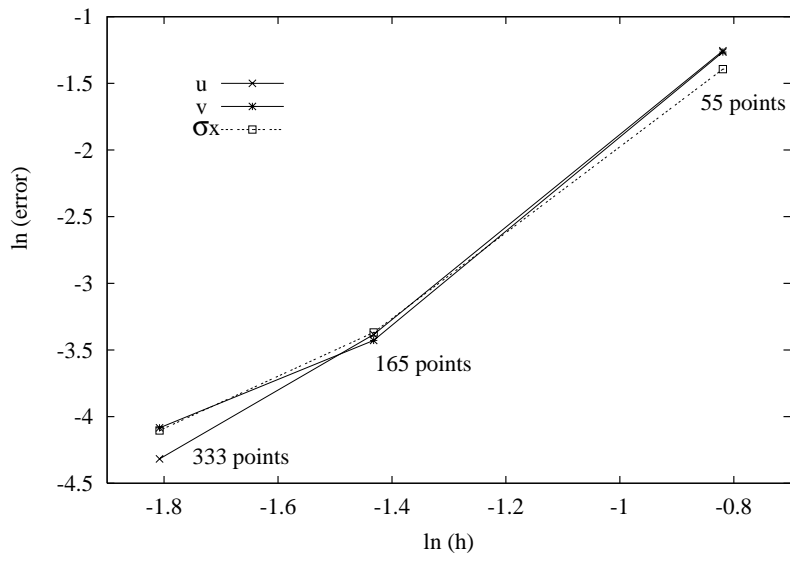
Figure 14: Cantilever beam with irregular distribution of points. Convergence of displacements and σ_x stress with the average radial distance for all clouds
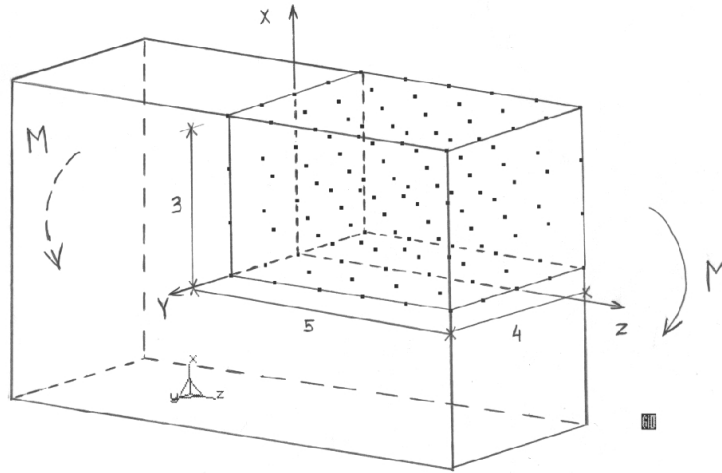

Figure 15: Prismatic solid under end bending moment. Geometry, loading and arrangement of points $E = 1000$, $\nu = 0.25$

	u	w	σ_z
FPM 120 points (regular grid)	-0.0138	0.015	3.0066
FPM 271 points (irregular grid)	-0.0139	0.014991	3.0086
Analytical [28]	-0.013625	0.015	3.0

Table 5: Numerical and analytical results for prismatic solid under end bending moment. Figures show maximum displacement and maximum stress values
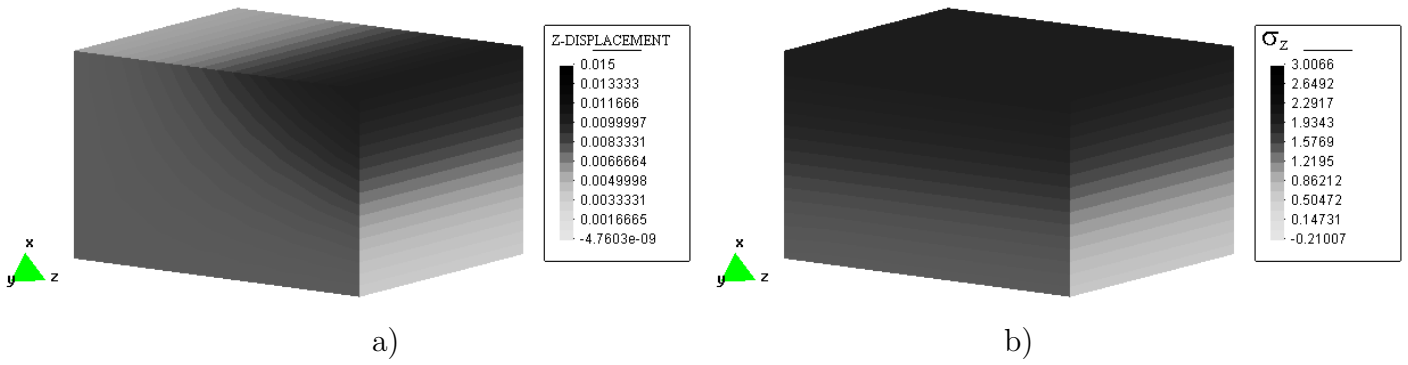
Figure 16: Prismatic solid under end bending moment analyzed with the stabilized FPM. a) Contours of z displacement; b) Contours of σ_z stress
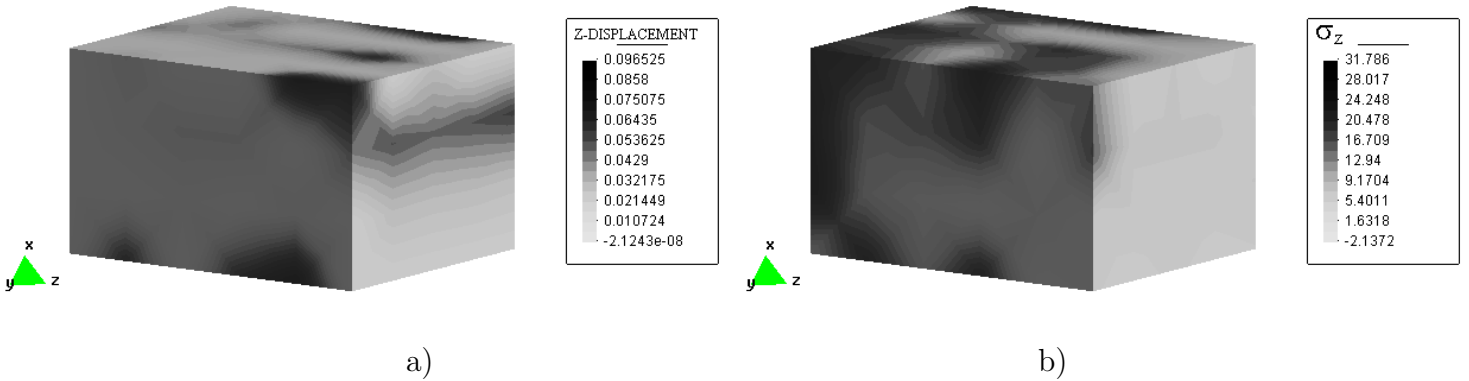

Figure 17: Prismatic solid under end bending moment analyzed with the FPM without the stabilization procedure. a) Contours of z displacement; b) Contours of σ_z stress

CONCLUSIONS

The stabilized FPM using the finite calculus procedure is a promising numerical method for the meshless solution of problems in solid mechanics. The stabilization terms were found to be crucial to obtain a smooth solution in all cases studied. Results for the 2D and 3D elasticity problems analyzed with the stabilized quadratic FPM yielded a higher accuracy than those obtained with standard FEM. The accuracy was remarkably higher for the stress values. The optimal selection of the stabilization parameters and the validation of the stabilized FPM for problems involving heterogeneous materials and complex 3D geometries are the main challenges in the extension and validation of the new meshless procedure.

ACKNOWLEDGEMENTS

References

[1] J.J. Monaghan. Smoothed particle hydrodynamics. *Annu. Rev. Astron. Physics*, **30**, 543–574, (1992).

[2] P.W. Randles and L.D. Libersky. Smoothed particle hydrodynamics: Some recent improvement and applications. *Appl. Mech. Engng.*, **139**, 1–4, 375, (1996).

[3] N. Perrone and R. Kao. A general finite difference method for arbitrary meshes. *Comp. Struct.*, **5**, 45-47, (1975).

[4] T. Liszka and J. Orkisz. The finite difference method at arbitrary irregular grids and its application in applied mechanics. *Comp. Struct.*, **11**, 83-95, (1980).

[5] B. Nayroles, G. Touzot and P. Villon. Generalizing the FEM: Diffuse approximation and diffuse elements. *Comput. Mechanics*, **10**, 307-18, (1992).

[6] T. Belytschko, Y. Lu and L. Gu. Element free Galerkin methods. *Int. J. Num. Meth. Engng.*, **37**, 229-56, (1994).

[7] J. Dolbow and T. Belytschko. An introduction to programming the meshless element free Galerkin method. *Archives of Comput. Meth. in Engng.*, **5** (3), 207–241, (1998).

[8] W.K. Liu, Y Chen, s. Jun, J.s. Chen, T. Belytschko, C. Pan, R.A. Uras and C.T. Chang. Overview and applications of the Reproducing Kernel particle method. *Archives of Comput. Meth. in Engng.*, Vol. **3**(1), 3–80, (1996).

[9] S.N. Atluri and T. Zhu. A new meshless local Petrov-Galerkin (MLPG) approach in computational mechanics. *Comput. Mech.*, **22**, 117–127, 1998.

[10] S.N. Atluri, H. Kim and J.Y. Cho. A critical assessment of the truly meshless local Petrov-Galerkin (MLPG) and local boundary integral equation (LBIE) methods. *Comput. Mech.*, **24**, 5, 348–373, 1999.

[11] S. De and K.J. Bathe. The method of finite spheres. *Computational Mechanics*, **25**, 329–345, 2000.

[12] E. Oñate, S. Idelsohn, O.C. Zienkiewicz and T. Fisher. A finite point method for analysis of fluid flow problems. *Proceedings of the 9th Int. Conference on Finite Element Methods in Fluids*, Venize, Italy, 15-21, October (1995).

[13] E. Oñate, S. Idelsohn, O.C. Zienkiewicz and R.L. Taylor. A finite point method in computational mechanics. Applications to convective transport and fluid flow. *Int. J. Num. Meth. Engng.*, Vol. **39**, 3839–3866, (1996).

[14] E. Oñate, S. Idelsohn, O.C. Zienkiewicz and R.L. Taylor. A stabilized finite point method for analysis of fluid mechanics problems. *Comput. Meth. in Appl. Engng.*, Vol. **139**, 1-4, pp. 315–347, (1996).

[15] E. Oñate and S. Idelsohn. A mesh free finite point method for advective-diffusive transport and fluid flow problems. *Computational Mechanics*, **21**, 283–292, (1988).

[16] E. Oñate, C. Sacco and S. Idelsohn. A finite point method for incompressible flow problems. *Comp. and Visual in Science*, **3**, 67–75, (2000).

[17] R.L. Taylor, S. Idelsohn, O.C. Zienkiewicz and E. Oñate. Moving least square approximations for solution of differential equations. *Research Report* 74, CIMNE, Barcelona, 1995.

[18] E. Oñate. Derivation of stabilized equations for advective-diffusive transport and fluid flow problems. *Comput. Meth. Appl. Mech. Engrg.*, Vol. 151, 1-2, pp. 233–267, (1998).

[19] E. Oñate, J. García and S. Idelsohn. Computation of the stabilization parameter for the finite element solution of advective-diffusive problems. *Int. J. Num. Meth. Fluids*, Vol. 25, pp. 1385–1407, (1997).

[20] E. Oñate, J. García and S. Idelsohn. An alpha-adaptive approach for stabilized finite element solution of advective-diffusive problems with sharp gradients. *New Advances in Adaptive Comp. Met. in Mech.*, P. Ladeveze and J.T. Oden (Eds.), Elsevier, (1998).

[21] E. Oñate and M. Manzan. A general procedure for deriving stabilized space-time finite element method for advective-diffusive problems. *Int. J. Num. Meth. Fluids*, **31**, 203–221. 1999.

[22] E. Oñate. A finite element method for incompressible viscous flows using a finite increment calculus formulation. *Comput. Methods Appl. Mech. Engrg.*, **182**, 355–370, 2000.

[23] E. Oñate and J. García. A stabilized finite element method for incompressible viscous flows with surface waves using a finite calculus procedure. *Comput. Methods Appl. Mech. Engrg.*. To appear

[24] E. Oñate, F. Perazzo and J. Miquel. Advances in the stabilized finite point method for structural mechanics. Publication No. 164, CIMNE, Barcelona, May 1999. Also in *European Conference on Computational Mechanics, (ECCM'99)*, August 31–September 3, 1999, Munich, Germany. Edited by W.Wunderlich *et al.*

[25] O.C. Zienkiewicz and R.L. Taylor. *The finite element method.* 5th Edition, 3 Volumes, Butterworth-Heinemann, 2000.

[26] S. Beissel and T. Belytschko. Nodal integration of the element-free Galerkin method. *Comput. Methods Appl. Mech. Engrg.*, **139**, 49–74, 1996.

[27] J. Bonet and S. Kulasegarm. Finite increment gradient stabilization of point integrated meshless method for elliptic equations. To be published in Communic. in Appl. Num. Meth. in Engng.

[28] S.P. Timoshenko and J.N. Goodier. *Theory of elasticity.* 3d. Edition, Mc-Graw Hill, (1970).